

Modeling non local thermodynamic equilibrium plasma using the Flexible Atomic Code data

Bo HAN^{1,2}, Feilu WANG¹, David SALZMANN³, Gang ZHAO¹

¹*Key laboratory of Optical Astronomy, National Astronomical Observatories,
Chinese Academy of Sciences, Beijing 100012, China*

²*University of Chinese Academy of Sciences, Beijing 100049, China*

³*Weizmann Institute of Science, Rehovot, Israel*

bhan@bao.ac.cn

(Received ; accepted)

Abstract

We present a new code, RCF(“Radiative-Collisional code based on FAC”), which is used to simulate steady-state plasmas under non local thermodynamic equilibrium condition, especially photoionization dominated plasmas. RCF takes almost all of the radiative and collisional atomic processes into rate equation to interpret the plasmas systematically. The Flexible Atomic Code (FAC) supplies all the atomic data RCF needed, which insures calculating completeness and consistency of atomic data. With four input parameters relating to the radiation source and target plasma, RCF calculates the population of levels and charge states, as well as potentially emission spectrum. In preliminary application, RCF successfully reproduces the results of a photoionization experiment with reliable atomic data. The effects of the most important atomic processes on the charge state distribution are also discussed.

Key words: atomic data — atomic processes — methods: numerical — plasmas

1. Introduction

Non local thermodynamic equilibrium (NLTE) exists in a wide variety of astrophysical and laboratory plasmas. Examples of NLTE astronomical plasmas are the stellar corona, interstellar nebulae and some other low density ionized plasmas. X-ray satellites, such as Chandra and XMM-Newton, provided large amount of high resolution spectra from astronomical objects, many of which are in NLTE. In laboratory, NLTE exists in laser produced plasmas, tokamaks and Z-pinch based experiments.

In the present paper, we introduce a new NLTE plasma computer code, which we called Radiative-Collisional code based on FAC (abbreviated RCF). RCF is a radiative-collisional

Table 1. Atomic processes in RCF (Salzmann 1998).

Reaction	Direct Process	Inverse Process
$X_{i,j} \rightleftharpoons X_{i,j'} + h\nu$	Spontaneous Decay	Photo excitation
$X_{i,j} + e \rightleftharpoons X_{i,j'} + e'$	Electron Impact Excitation	Electron Impact Deexcitation
$X_{i,j} + h\nu \rightleftharpoons X_{i+1,j'} + e$	Photoionization	Radiative Recombination
$X_{i,j} + e \rightleftharpoons X_{i+1,j'} + e' + e''$	Electron Impact Ionization	Three-Body Recombination
$X_{i,j} \rightleftharpoons X_{i+1,j'} + e$	Autoionization	Dieletronic Captrue

code that includes photoionization as well, thereby it is appropriate especially to astrophysical plasmas. In the following we show its accuracy relative to other codes.

Several similar codes, which are being used for analysis of astrophysical spectra, have already been published in the literature. Examples are GALAXY (Rose 1998, Foord et al. 2004, Foord et al. 2006, Rose et al. 2004), NIMP (Djaoui & Rose 1992, Rose et al. 2004), FLYCHK (Chung et al. 2003), CLOUDY (Ferland et al. 1998), XSTAR (Kallman et al. 1996, Kallman et al. 2004, Kallman & Bautista 2001, Bautista & Kallman 2001, Boroson et al. 2003), PhiCRE (Salzmann et al. 2011, Wang et al. 2011) and SASAL (Liang et al. 2014). Some of these codes are used to interpret laboratory experiments (GALAXY, FLYCHK, NIMP and PhiCRE), while others are used in analysis of astrophysical spectra (CLOUDY and XSTAR), while RCF is designed to be applicable to both of the conditions above.

The aim of this paper is to give a detail introduction of RCF and to present its application to a photoionization experiment. Section 2 presents the model and the method of to calculate the atomic rate coefficients. In section 3, we apply RCF to reproduce the iron charge state distribution of a photoionization experiment, together with a discussion of the importance of the various atomic processes. A short summary is given in the last section.

2. Rate equation and Atomic Data

2.1. Rate Equation

RCF is a steady-state collisional-radiative optically-thin model. Its rate-equation (Salzmann 1998) is

$$\frac{dN_{i,j}}{dt} = \text{populating processes} - \text{depopulating processes} = 0 \quad (1)$$

where $N_{i,j}$ is the density of the j th level of the i th charge state. The processes included are the ionization and recombination between neighboring charge states and excitation and de-excitation within the same charge state. Their inverse processes are also taken into account by detailed balance principle. The processes included in Eq.(1) are listed in Table 1.

2.2. Atomic Data and Reaction Rates

The atomic data for RCF are calculated by FAC (Gu 2008). FAC is a fully relativistic software package that computes various atomic data, which has been widely used in astrophysical and laboratory research (Gu 2008). With the ions and their configurations as input, the SFAC interface can supply $j - j$ coupled energy levels ($E_{i,j}$), bound-bound spontaneous decay rates ($A_{i,j \rightarrow j'}$), bound-bound electron-collision excitation (CE) cross sections (σ_{CE}), bound-free photoionization (PI) and electron-impact ionization (EI) cross sections (σ_{PI}, σ_{EI}), autoionization rate (AI) (R_{AI}), and free-bound radiative recombination (RR) cross section (σ_{RR}), where σ_{PI} and σ_{RR} are related through the Milne relation.

The processes in Table 1 can be divided into two kinds, the inherent reactions inside the plasma and the reactions driven by an external radiation field.

The inherent ones include the reactions between ions and electrons driven by collision, and spontaneous decay inside all ions. The solar corona plasma is believed to be dominated by these processes. In such low density plasma, the dominant processes are spontaneous decay and radiative recombination, whose rates are much higher than collisional decay and three-body recombination. As a result, the plasma departs from the local thermodynamic equilibrium, and can no longer be described by Saha and Boltzmann equations. The collisions between particles cause energy exchange and state distribution changes. Usually charge exchange reactions between ions have negligibly low probabilities (Salzmann 1998).

The rate per volume of electron impact excitation reaction is calculated by

$$\frac{\text{reactions}}{\text{cm}^3\text{s}} = N_{i,j}n_e\mathcal{E}_c, \quad (2)$$

where n_e is the electron density in plasma, and $\mathcal{E}_c(\text{cm}^3\text{s}^{-1})$ is the collisional excitation rate coefficient. The rate coefficient of collisional excitation is given by

$$\mathcal{E}_c = \int_{\Delta E}^{+\infty} f(v)\sigma_{CE}(v)dv, \quad (3)$$

where $f(v)$ is velocity distribution of electrons, assumed to have Maxwellian distribution with electron temperature T_e , $\sigma_{CE}(v)$ is the collisional excitation cross section from $X_{i,j}$ to $X_{i,j'}$ at velocity v , and ΔE is the excitation energy. Thus, the CE rate coefficient expressed in term of incident electron energy is

$$\mathcal{E}_c = \sqrt{\frac{8}{\pi m_e T_e^3}} \int_{\Delta E}^{+\infty} E\sigma_{CE}(E)\exp\left(-\frac{E}{T_e}\right)dE, \quad (4)$$

where E is incident electron energy, m_e is the mass of electron, and $\sigma_{CE}(E)$ is the collisional excitation cross section calculated by FAC.

The calculations of collisional ionization and radiative recombination rates have a similar form with CE. The CI and RR rate coefficients (cm^3s^{-1}) are

$$\mathcal{I}_c = \sqrt{\frac{8}{\pi m_e T_e^3}} \int_{\Delta E}^{+\infty} E\sigma_{CI}(E)\exp\left(-\frac{E}{T_e}\right)dE, \quad (5)$$

$$\mathcal{R}_r = \sqrt{\frac{8}{\pi m_e T_e^3}} \int_0^{+\infty} E \sigma_{RR}(E) \exp\left(-\frac{E}{T_e}\right) dE, \quad (6)$$

where $\sigma_{CI}(E)$ is the CI cross section from $X_{i,j}$ to $X_{i+1,j'}$ and $\sigma_{RR}(E)$ is the RR cross section from $X_{i+1,j''}$ to $X_{i,j}$.

The inverse process to CI is three-body recombination from $X_{i+1,j''}$ to $X_{i,j}$ and CE's inverse process is collisional deexcitation from $X_{i,j'}$ to $X_{i,j}$. Their rate coefficients are obtained by Detailed Balance Principle

$$\mathcal{R}_t = \frac{1}{2} \left(\frac{2\pi \hbar^2}{m_e T_e} \right)^{3/2} \frac{g_{i,j}}{g_{i+1,j'}} \exp\left(\frac{\Delta E}{T_e}\right) \mathcal{I}_c, \quad (7)$$

$$\mathcal{D}_c = \frac{g_{i,j}}{g_{i,j''}} \exp\left(\frac{\Delta E}{T_e}\right) \mathcal{E}_c, \quad (8)$$

It should be mentioned that the three body recombination rate coefficient, being dependent on two electrons, is proportional to n_e^2 ,

$$\frac{\text{reactions}}{\text{cm}^3 \text{s}} = N_{i,j} n_e^2 \mathcal{R}_t, \quad (9)$$

and the unit of \mathcal{R}_t is $\text{cm}^6 \text{s}^{-1}$.

The spontaneous processes in plasma are radiative decay and autoionization. Their rates are directly given by FAC, $A_{i,j \rightarrow j'}(\text{s}^{-1})$ and $R_{AI}(\text{s}^{-1})$. Radiative decay process is the mechanism of plasma emitting line spectrum. In the present work, we assume that the photons emitted by radiative decay are not reabsorbed. Autoionization occurs in case of doubly excited ions, and is possible only if the sum of the energies of the two electrons is higher than the binding energy of the ion. During autoionization, the energy, which is released by the inner excited electrons decays to a lower state, ionizes the outer one into the continuum. There are several ways to produce such highly excited ions, such as dielectron capture, photoexcitation and photoionization of inner-shell electrons, and the two inner-shell processes are especially important in conditions where strong fields exist. Dielectronic capture into doubly excited states is the inverse process of autoionization, and its rate coefficient ($\text{cm}^3 \text{s}^{-1}$) is obtained by the detailed balance principle,

$$\mathcal{R}_d = \frac{1}{2} \left(\frac{2\pi \hbar^2}{m_e T_e} \right)^{3/2} \frac{g_{i,j}}{g_{i+1,j'}} \exp\left(\frac{\Delta E}{T_e}\right) R_{AI}. \quad (10)$$

The rate coefficient of dielectronic recombination is obtained when Eq.(10) is multiplied by the branching ratio for radiative stabilization of the doubly excited state, $A_{i,j}/(\sum A_{i,j} + \sum R_{AI})$ (Salzmann 1998).

When the plasma is irradiated by a strong external radiation source, the radiative field will excite or ionize the ions causing the plasma gets into photoionizational collisional radiative equilibrium regime. In this case, the photoionization and photoexcitation processes are not negligible and may dominate the charge state distribution. For example, the strong radiation

field emitted by an accreting compact object is believed to be the main ionization mechanism of the highly ionized low density gas around it.

The photoionization reaction rate per unit volume is calculated by

$$\frac{\text{reactions}}{\text{cm}^3 \text{s}} = N_{i,j} R_{PI} = N_{i,j} \int_{\Delta E}^{+\infty} n_p(h\nu) c \sigma_{PI}(h\nu) d(h\nu),$$

where R_{PI} is the photoionization rate (s^{-1}), ΔE is the ionizing energy from $X_{i,j}$ to $X_{i+1,j'}$, $h\nu$ is the energy of incident photon, $\sigma_{PI}(h\nu)$ is the photoionization cross section, c is the speed of light, and $n_p(h\nu) d(h\nu)$ is the density of photons having energy in the range $[h\nu, h\nu + d(h\nu)]$. For a black body radiation source having radiation temperature T_r , with energy intensity $I(h\nu)$ ($\text{eV}/(\text{cm}^2 \cdot \text{s} \cdot \text{eV})$) and dilution factor α , $n_p(h\nu) = (\alpha I(h\nu))/(ch\nu)$, then R_{PI} becomes

$$R_{PI} = \alpha \int_{\Delta E}^{+\infty} \frac{I(h\nu)}{h\nu} \sigma_{PI}(h\nu) d(h\nu), \quad (11)$$

The photoexcitation rate per volume from $X_{i,j}$ to $X_{i,j'}$ is

$$\frac{\text{reactions}}{\text{cm}^3 \text{s}} = N_{i,j} R_{PE} = N_{i,j} h J(h\nu) B_{i,j \rightarrow j'}, \quad (12)$$

$B_{i,j \rightarrow j'}$ is the Einstein B -coefficient The photo-excitation rate (s^{-1}) irradiated by a diluted isotropical black body radiation source is

$$R_{PE} = \alpha I(h\nu) \frac{g_{j'}}{g_j} \frac{h^2 c^2}{2(h\nu)^3} A_{i,j' \rightarrow j}, \quad (13)$$

Currently, RCF is assumes a blackbody radiator, thereby the photoionization and photoexcitation rate are

$$R_{PI} = \alpha \frac{2}{h^3 c^2} \int_{\Delta E}^{+\infty} \frac{(h\nu)^2}{e^{\frac{h\nu}{T_r}} - 1} d(h\nu), \quad (14)$$

$$R_{PE} = \alpha \frac{g_{j'}}{g_j} A_{i,j' \rightarrow j} \frac{1}{e^{\frac{h\nu}{T_r}} - 1}, \quad (15)$$

2.3. Input Parameters

These equations require four input parameters in RCF, which are radiation temperature T_r , dilution factor α , electron temperature T_e , and electron density n_e . T_r is the temperature of the blackbody radiation source. α stands for the attenuation of radiation between the source and the irradiated plasma, and it mainly depends on the opacity and distance. T_e and n_e are the properties of the irradiated plasma, and they are sufficient to describe plasma under coronal equilibrium. However, when the external radiation field is important, all the four input parameters are needed.

In experiments these parameters are measured directly or deduced indirectly from some measured values. However, depending on the experiment setup, some parameters cannot be obtained. For example, the experiment by Fujioka et al. (2009) with silicon target provided all four parameters with some uncertainties, whereas T_e does not have a definite value in the Sandia experiment by Foord et al. (2004) with iron target. In astrophysics, T_r is estimated by the

observed continuum spectrum, and α is roughly deduced from the distance between two celestial objects by the inverse square law. Usually, T_e and n_e of the irradiated plasma are deduced from some characteristic spectral line ratios. For example, the ratios of resonance, intercombination and forbidden lines of He-like ions are important diagnostics of electron density and temperature (Porquet & Dubau 2000). The radiative recombination continuum (RRC) is also an important method to diagnose electron temperature of plasmas.

3. Simulation of Sandia Photoionization Experiment

Photoionized plasma is a special kind of NLTE plasma. It is widely observed in the universe, such as low density nebula near accreting X-ray source. Recently, this kind of plasmas were also produced in laboratory using high power laser (Fujioka et al. 2009) and Z-pinch (Foord et al. 2004).

In this section, RCF is applied to the photoionization experiment at Sandia National Laboratory Z-facility (Foord et al. 2004). In this experiment, a 165 eV near-blackbody radiation source was created to produce a $n_e = 2 \pm 0.7 \times 10^{19} \text{cm}^{-3}$ plasma (Foord et al. 2004) in photoionizational collisional radiative equilibrium regime (Wang et al. 2011). A distribution of iron charge states was deduced from the absorption spectrum. A number of papers (Foord et al. 2004, Foord et al. 2006, Wang et al. 2011, Han et al. 2013, Liang et al. 2014) tried reproducing the measured charge state distribution using different models and computer codes. All these works assumed a steady state photoionized plasma, which is also adopted by RCF.

In this experiment, only two of the parameters needed in RCF are specified, which are T_r and n_e . T_e is a disputed focus of the former works, and it spans from 70 eV to 150 eV in different models (Foord et al. 2006, Wang et al. 2011). However, α was not specified by some models (Foord et al. 2006), although it is an important parameter that controls the influence of radiative field on the plasma (Han et al. 2013). Fortunately, the experiment yielded an ionization parameter $\xi_{exp} = 25 \text{ erg} \cdot \text{cm} \cdot \text{s}^{-1}$ (Foord et al. 2004) at the peak of the radiation pulse. ξ is a parameter related to the radiation field $\xi = 16\pi^2 J/n_e$, and for an isotropic blackbody radiation field $\xi = 16\pi\sigma T_r^4/n_e$, where J is the mean intensity and σ is the Stefan-Boltzmann constant. Therefore, the ratio between experimental value and theoretical value stands for the attenuation of the radiative field, ie. $\alpha = \xi_{exp}/\xi_{theo}$, which can be derived as $\alpha = 0.85\% - 1.76\%$.

Figure 1 displays the charge state distribution of the iron photoionization experiment predicted by RCF and comparisons with the experiment values and some previous works (Foord et al. 2006, Wang et al. 2011). Seemingly, RCF produces the result closest to the experiment, and almost every ion is within the experiment uncertainties. The average charge state in present calculation is $\langle Z \rangle = 16.12$, which agrees well with the measured value $\langle Z \rangle = 16.1 \pm 0.2$. The input parameters used here are $T_r=165 \text{ eV}$, $n_e = 2 \times 10^{19} \text{cm}^{-3}$, $\alpha = 1.4\%$ and $T_e = 150 \text{ eV}$. $T_e=150 \text{ eV}$ agrees with CLOUDY and FLYCHK, and some other works, such as NIMP (Rose et al. 2004) and Han et al. (2013). $\alpha = 1.4\%$ is in the interval deduced above.

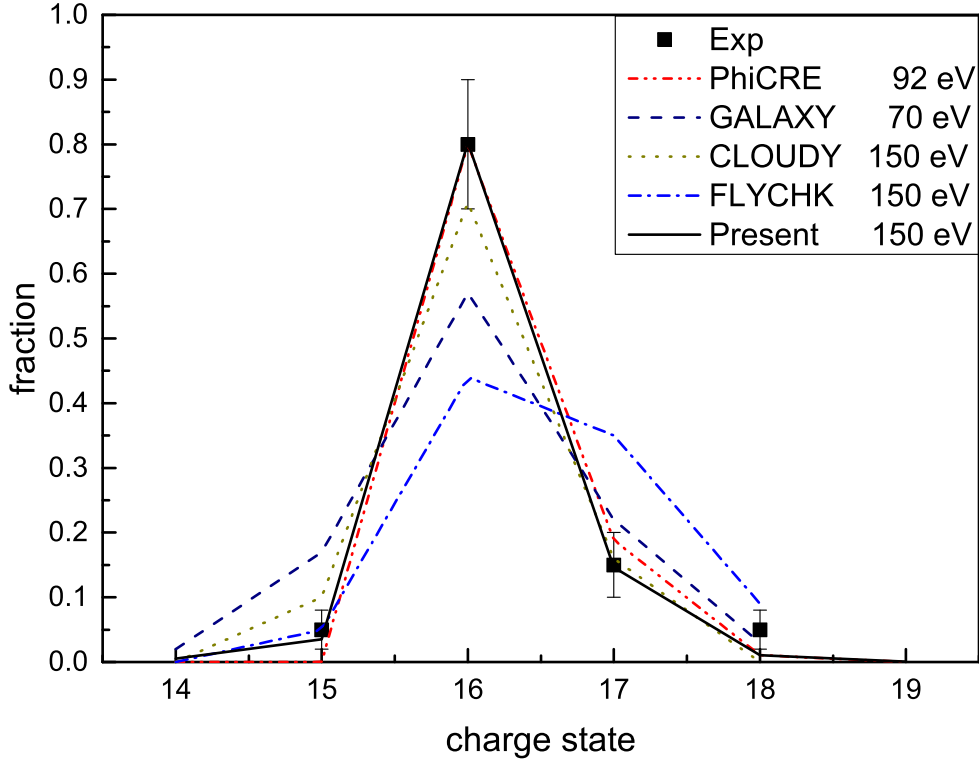


Fig. 1. The charge state distribution calculated by RCF (Solid) for Fe photoionization experiment(Scatters), and comparison with PhiCRE (Dash Dot Dot), GALAXY (Dash), CLOUDY (Dot), and FLYCHK (Dash Dot) (Foord et al. 2006, Wang et al. 2011). The temperatures are electron temperatures used by these models.

A main reason of the differences among the codes in Figure 1 is the different sources of atomic data. GALAXY employs an average-of-configuration approximation for electronic states, screened hydrogenic for both collisional and radiative processes, and Hartree-Dirac-Slater or Kramers cross sections for photoionization (Rose 1998, Foord et al. 2006). FLYCHK uses hydrogenic approximation to calculate energy levels and level populations (Chung et al. 2003, Foord et al. 2006). Results of GALAXY and FLYCHK largely deviate from the measured one. The atomic databases of CLOUDY are accurate enough to be comparable with spectral emission data (Ferland et al. 1998, Foord et al. 2006), but there still are some obvious disparities between it and the experiment. The energy levels and spontaneous decay rates of PhiCRE are taken from the NIST database, and other rate coefficients are calculated by widely used formulas (Salzmann et al. 2011, Wang et al. 2011).

The atomic data of RCF are calculated by FAC, which calculates all the atomic data by a fully relativistic approach based on Dirac equation (Gu 2008), and this single theoretical

framework ensures self-consistency between different parts. The configurations calculated with FAC of present work are listed Table 2, which include 1948 singly or doubly excited levels. For saving computation time, the maximum principle quantum number n is set to be 4. Because the states with K-shell vacancies have energies higher than 7 keV, which are much higher than the energies of photons and electrons under this experiment condition, K-shell is closed in FAC calculation. For ensuring the accuracy of present work, we compare the present FAC data with some literature values. Table 3 is the comparison of energy levels for $2s^22p^53l$ and $2s2p^63l$ states of Fe^{16+} between the NIST database (Kramida et al. 2014) and present work, and it shows excellent agreement (within 0.4%). Figure 2 shows the comparison of radiative decay rates (s^{-1}) between present work and the available corresponding transitions on the NIST database (Kramida et al. 2014) of the four most abundant charge states. As shown, there are more than 80% of present data within 20% agreement with NIST database (Kramida et al. 2014). According to Eq.(14), the accuracy of radiative decay rates also guarantees the calculating of photoexcitation rates. For collisional excitation, Figure 3 is the comparison of cross section of Fe^{15+} and Fe^{16+} for transitions from their ground states to their first excited levels. The present FAC results agree well with those calculated with ICFT (intermediate-coupling frame transformation) R-matrix (Liang et al. 2009, Liang & Badnell 2010) and Dirac R-matrix (Aggarwal et al. 2003). Using these data, RCF successfully reproduces the experiment result, and we look forward to applying it to spectral analysis of laboratory or astrophysical plasmas in future works.

1336:

1336:

In Figure 4, we compare the influences of some important processes on the experimental results. Case A is the one presented in Figure 1, in which we included all the relevant processes in RCF and all the configurations in Table 2.

Case B uses data without the doubly excited levels in Table 2. As can be seen, there are significant differences relative to Case A.

In Case C both the autoionization and its inverse process, dielectronic capture, are turned off. Results of Case C are close to those of Case B, and both predict an average charge lower than that of Case A. This means that doubly excited states are non-ignorable in the current calculation of charge state distributions. In other words, autoionization is an important ionizing channel, and doubly excited states act like ladders to the next charge state in this experiment.

In Cases D and E, we examine the influence of the radiation field on the Sandia experiment charge state distribution. First we note that there is a big difference between the binding energy of the two most important charge states in the experiment: the ionization energy of Fe^{15+} (Na-like) is 489.312 eV, and that of Fe^{16+} (Ne-like) is 1262.7 eV. As shown in Figure 5, a larger fraction of photons than electrons has sufficient energy to excite or ionize Fe^{+15} and Fe^{+16} . In fact, we have found that the influence of electron collisional ionization is so small

Table 2. The configurations used by Case A.

Charge State	Singly Excited			Doubly Excited	
Fe^{14+}	$2s^2 2p^6 3s^2$	$2s^2 2p^6 3s 3p$	$2s^2 2p^6 3p^2$	$2s^2 2p^5 3s^2 3p$	$2s 2p^6 3s^2 3p$
	$2s^2 2p^6 3s 3d$	$2s^2 2p^6 3p 3d$	$2s^2 2p^6 3d^2$		
	$2s^2 2p^6 3s 4s$	$2s^2 2p^6 3s 4p$	$2s^2 2p^6 3s 4d$		
	$2s^2 2p^6 3s 4f$				
Fe^{15+}	$2s^2 2p^6 3s$	$2s^2 2p^6 3p$	$2s^2 2p^6 3d$	$2s^2 2p^5 3s^2$	$2s^2 2p^5 3s 3p$
	$2s^2 2p^6 4s$	$2s^2 2p^6 4p$	$2s^2 2p^6 4d$	$2s^2 2p^5 3p^2$	$2s^2 2p^5 3s 3d$
	$2s^2 2p^6 4f$			$2s^2 2p^5 3p 3d$	$2s^2 2p^5 3d^2$
				$2s 2p^6 3s^2$	$2s 2p^6 3s 3p$
				$2s 2p^6 3p^2$	$2s 2p^6 3s 3d$
				$2s 2p^6 3p 3d$	$2s 2p^6 3d^2$
Fe^{16+}	$2s^2 2p^6$	$2s^2 2p^5 3s$	$2s^2 2p^5 3p$	$2s 2p^5 3s^2$	$2s 2p^5 3s 3p$
	$2s^2 2p^5 3d$	$2s 2p^6 3s$	$2s 2p^6 3p$	$2s 2p^5 3p^2$	$2s 2p^5 3s 3d$
	$2s 2p^6 3d$	$2s^2 2p^5 4s$	$2s^2 2p^5 4p$	$2s 2p^5 3p 3d$	$2s 2p^5 3d^2$
	$2s^2 2p^5 4d$	$2s^2 2p^5 4f$			
Fe^{17+}	$2s^2 2p^5$	$2s 2p^6$	$2s^2 2^4 3s$	$2s 2p^4 3s^2$	$2s 2p^4 3s 3p$
	$2s^2 2^4 3p$	$2s^2 2^4 3d$	$2s 2p^5 3s$	$2s 2p^4 3p^2$	$2s 2p^4 3s 3d$
	$2s 2p^5 3p$	$2s 2p^5 3d$	$2s^2 2^4 4s$	$2s 2p^4 3p 3d$	$2s 2p^4 3d^2$
	$2s^2 2^4 4p$	$2s^2 2^4 4d$	$2s^2 2^4 4f$		
	$2s^2 2^4 4s$	$2s^2 2^4 4p$	$2s^2 2^4 4d$		
	$2s^2 2^4 4f$				
Fe^{18+}	$2s^2 2p^4$	$2s 2p^5$	$2p^6$		
	$2s^2 2p^3 3s$	$2s 2p^4 3s$			
Fe^{19+}	$2s^2 3p^3$				

that its omission from the computations is hardly different from Case A.

There are two radiation driven processes in the code, photoexcitation (PE) and photoionization (PI). PE is omitted in Case D, whereas PI is turned off in Case E. It can be seen from Figure 4 that the absence of PE significantly reduces the average charge state, *i.e.*, photoexcited states play an important role in the charge state distribution. Case E is very close to Case A. The reason for this behavior is the large difference between the binding energies of Fe^{+15} and Fe^{+16} . On the other hand, there is a threshold between Fe^{16+} and Fe^{17+} , because neon-like Fe^{+16} has a closed shell stable configuration.

Both of PE and PI have preference to ionize inner-shell electrons resulting in autoionizing states. However, according to the photon energy distribution in Figure 5 and the energy levels of main ions, the doubly excited levels seem to be more likely produced by PE process. Actually, when the PE channel to doubly excited states is shut down, the result is almost the same as

Table 3. Comparison of energy levels for $2s^22p^53l$ and $2s2p^63l$ states of Fe^{16+} between NIST and present work.

Index	Level		NIST	Present
0	$2s^22p^6$	1S_0	0	0
1	$2s^22p^53s$	3P_2	725.2443	723.9074
2		1P_1	727.1388	725.874
3	$2s^22p^53s$	3P_0	737.856	736.5231
4		3P_1	739.0537	737.762
5	$2s^22p^53p$	3S_1	755.4915	755.008
6	$2s^22p^53p$	3D_2	758.9928	757.7623
7		3D_3	760.6095	759.327
8		3D_1	771.0614	769.7896
9	$2s^22p^53p$	1P_1	761.7403	760.5093
10	$2s^22p^53p$	3P_2	763.5529	762.2596
11		3P_0	768.981	767.8495
12		3P_1	774.3073	773.1159
13	$2s^22p^53p$	1D_2	774.6855	773.415
14	$2s^22p^53p$	1S_0	787.7224	790.3189
15	$2s^22p^53d$	3P_0	801.4313	800.4122
16		3P_1	802.401	801.3396
17		3P_2	804.211	803.0749
18	$2s^22p^53d$	3F_4	804.2644	802.9189
19		3F_3	805.0331	803.6367
20		3F_2	817.5964	816.2671
21	$2s^22p^53d$	1D_2	806.728	805.3275
22	$2s^22p^53d$	3D_3	807.8004	806.4032
23		3D_1	812.369	811.2368
24		3D_2	818.4135	817.0462
25	$2s^22p^53d$	1F_3	818.9342	817.4908
26	$2s^22p^53d$	1P_1	825.7	825.4368
27	$2s2p^63s$	1S_0	869.1	867.1547
28	$2s2p^63p$	3P_1	892.55	892.5898
29	$2s2p^63p$	1P_1	896.939	895.3807

Case D, which confirms that PE is the main pumping mechanism of doubly excited states. Case E indicates that PE+AI process wins the competition in ionizing Fe^{15+} , but for Fe^{16+} the PI channel is important, too.

In Case F, collisional excitation (CE) is omitted, and it gets a strange result. The deletion of CE does not lower $\langle Z \rangle$ as Case D, but rather the plasma is more ionized than

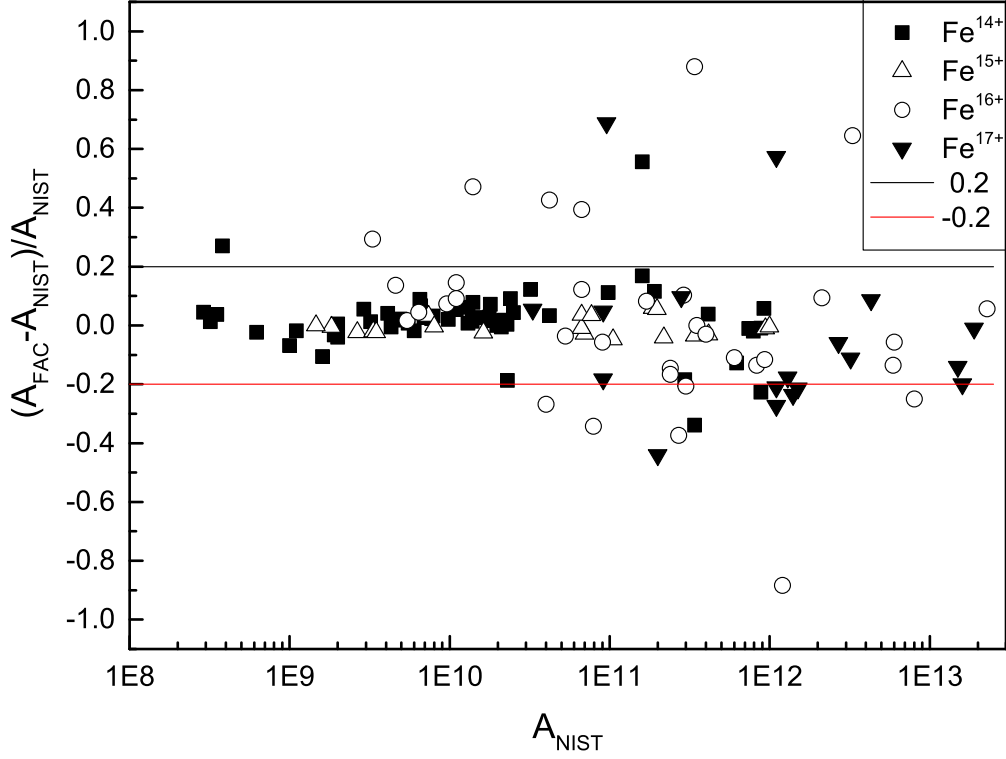


Fig. 2. Comparison of radiative decay rates between present work and corresponding available data on NIST from Fe^{14+} to Fe^{17+} .

Case A. According to Figure 5, although the electrons have comparatively lower energy and cannot ionize the ions as effectively as photons, they still can excite the ions to singly excited levels by collision. However, the collision produced singly excited levels have smaller reaction cross sections with photons than the ground state and lower levels, namely, they are more difficult to be ionized by photons. Therefore, the electrons certainly would take part in the competition of reacting with the ground state of ions, and as a result reducing the ionizing efficiency of PI and PE+AI. What is more, when the CE channel from the ground states of ions to the singly excited states is shut down, it produces a result similar to Case F, which confirms the discussion above. So that, it makes sense that why $\langle Z \rangle$ rises when CE is shut down.

In conclusion, RCF has a good agreement to the photoionization experiment results (Foord et al. 2004), and gives reasonable explanation for the charge state distribution. In the calculations of RCF, the charge state distribution of this experiment is a composite result of different atomic processes. The external field dominates the ionizations in the plasma by photoionization directly and photoexcitation plus autoionization indirectly. The transitions

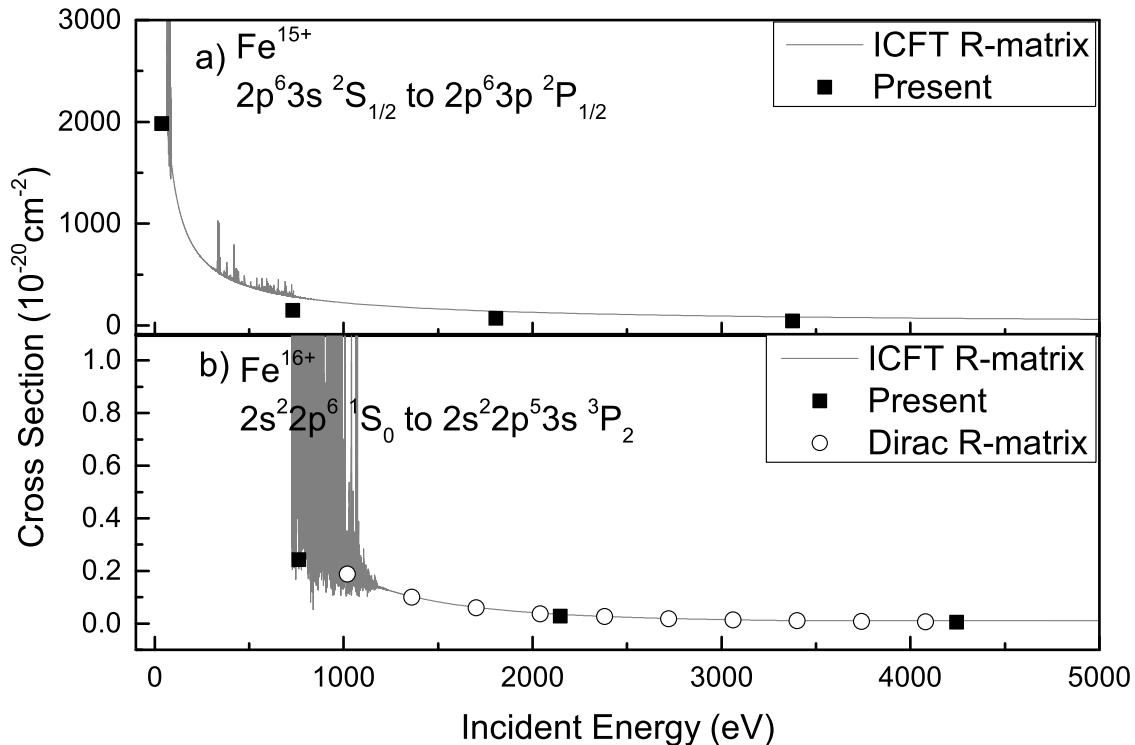


Fig. 3. Comparison of collisional excitation cross sections. (a) Transition from $2p^63s\ ^2S_{1/2}$ to $2p^63p\ ^2P_{1/2}$ of Fe^{15+} . Grey solid: ICFT R-matrix (Liang et al. 2009), black square: present FAC. (b) Transition from $2s^22p^6\ ^1S_0$ to $2s^22p^53s\ ^3P_2$ of Fe^{16+} . Grey solid: (Liang & Badnell 2010), black square: present FAC, circle: Dirac R-matrix (Aggarwal et al. 2003).

within any given single charge state can significantly affect the charge state distribution, and one of the interesting results of our computations is the role played by collisional excitation in this experiment, in which it reduces the total ionization rate by competing with PE and PI.

4. Summary

In this paper we introduced a new code, RCF, which is applied to plasma in NLTE condition, especially in the photoionization dominating regime. This code can calculate the level population, charge state distribution and spectra of a plasma in steady state. The atomic data source of this code is FAC, which is an easy to use and powerful software package to calculate various atomic data. The SFAC interface can provide all the atomic data needed in RCF, without any additional modifications. FAC is based on a fully relativistic theoretical framework, which ensures the accuracy and consistency of the atomic data.

All the plasma processes and their inverse ones are related by the detailed balance prin-

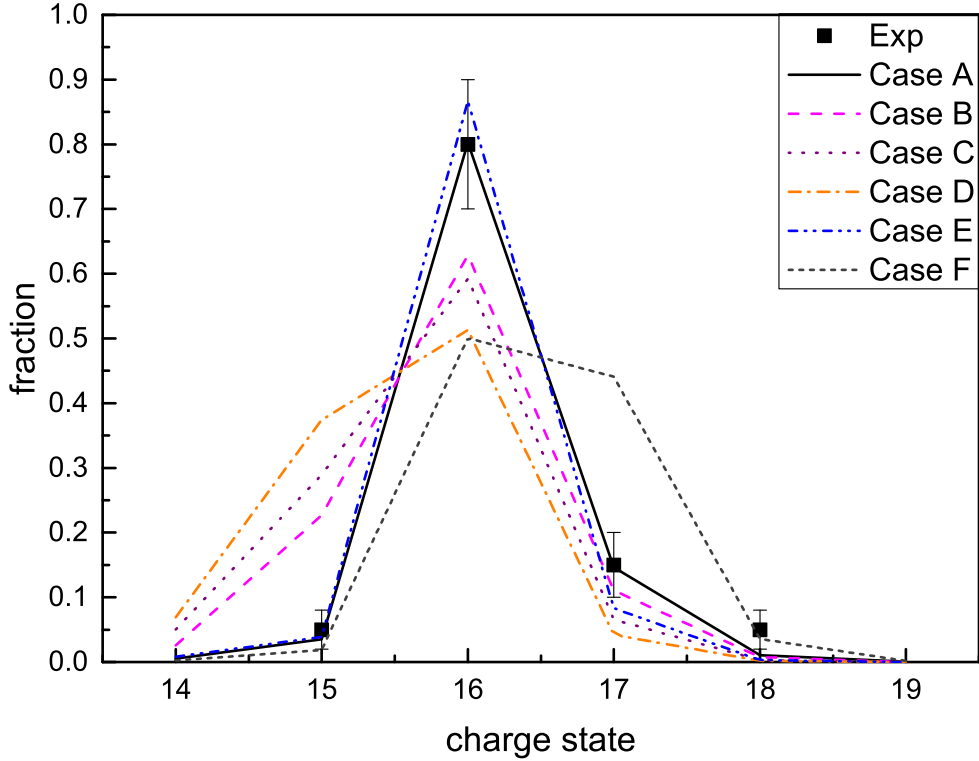


Fig. 4. The charge state distribution calculated by RCF with different data or without specific processes. Case A uses data with inner-shell holes (Solid), Case B use data without inner-shell holes (Dash). Case C (Dot), D (Dash Dot), E (Dash Dot Dot) use the same data as Case A, but there are no AI and DC processes in Case C, no PE process in Case D, no PI process in Case E, no CE process in Case F. The scatters are experiment values.

ciple in RCF. As a result, in high density regime, the RCF generates results similar to the Saha equation with same atomic data. In other words, RCF converges to LTE approximation under the appropriate condition. In radiation dominant regimes, RCF gets a charge state distribution which closely agrees to the results of the Fe photoionization experiment. A comparison is given to the results of other similar codes. We also discussed the influence of the various atomic processes to the charge state distribution of this experiment. Photoionization is not the only important ionizing channel, but the photoexcitation plus autoionization process are proved to be also significant. Although the electrons have comparatively lower energy than the photons, they still are important. The electrons can excite the ions to the levels which have small reaction cross sections for the photons, and the result is reducing the ionizing efficiency of the photons.

The charge state and levels' distributions are a prerequisite for the simulation of the

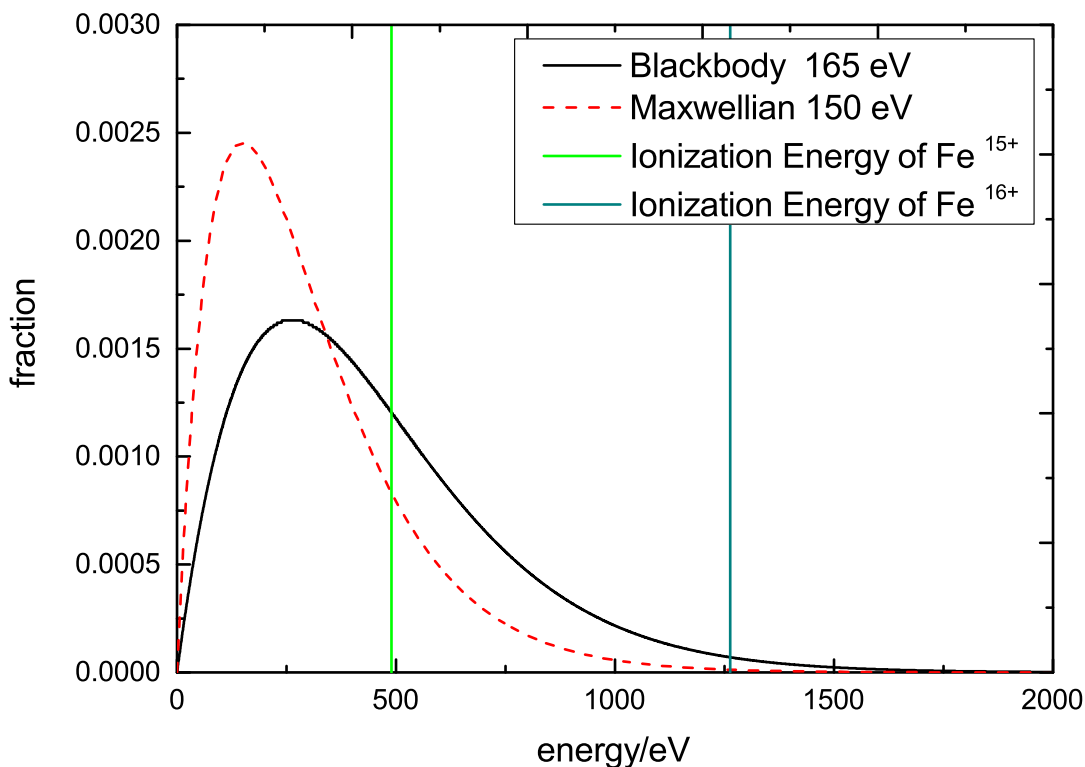


Fig. 5. The distribution of 165 eV blackbody photons (solid) and 150 eV Maxwellian electrons (dash).

emission spectrum, and we showed that all the atomic processes may have significant effect under the appropriate conditions. In particular, in the analysis of X-ray spectrum from a compact object photoexcitation is an important pumping mechanism (Kallman et al. 2014). Porquet & Dubau (2004) also emphasized the influence of cascading decay from higher levels and collisional excitation on the line ratios in plasma diagnosis. According to the result shown, RCF is a reasonable code to get accurate distributions in steady NLTE plasma by including all the processes and using FAC data. We shall use it for spectrum analysis in astrophysics and laboratory of photoionizing and collisional NLTE plasmas in our further works.

Acknowledgement

This work is supported by the NSFC under grants Nos.11173032 and 11135012, and by the National Basic Research Program of China (973 Program) under grant No.2013CBA01503.

References

- Aggarwal, K. M., Keenan, F. P., & Msezane, A. Z. 2003, *ApJS*, 144, 169
- Bautista, M. A., & Kallman, T. R. 2001, *ApJS*, 134, 139
- Boroson, B., Vrtilik, S. D., Kallman, T., & Corcoran, M. 2003, *ApJ*, 592, 516
- Chung, H.-K., Morgan, W. L., & Lee, R. W. 2003, *J. Quant. Spectrosc. Radiat. Transfer*, 81, 107
- Djaoui, A., & Rose, S. J. 1992, *Journal of Physics B Atomic Molecular Physics*, 25, 2745
- Ferland, G. J., Korista, K. T., Verner, D. A., et al. 1998, *PASP*, 110, 761
- Foord, M. E., Heeter, R. F., van Hoof, P. A., et al. 2004, *Physical Review Letters*, 93, 055002
- Foord, M. E., Heeter, R. F., Chung, H.-K., et al. 2006, *J. Quant. Spectrosc. Radiat. Transfer*, 99, 712
- Fujioka, S., Takabe, H., Yamamoto, N., et al. 2009, *Nature Physics*, 5, 821
- Gu, M. F. 2008, *Canadian Journal of Physics*, 86, 675
- Han, X.-Y., Wang, F.-L., Wu, Z.-Q., Yan, J., & Zhao, G. 2013, *Journal of the Physical Society of Japan*, 82, 024501
- Kallman, T. R., Liedahl, D., Osterheld, A., Goldstein, W., & Kahn, S. 1996, *ApJ*, 465, 994
- Kallman, T., & Bautista, M. 2001, *ApJS*, 133, 221
- Kallman, T. R., Palmeri, P., Bautista, M. A., Mendoza, C., & Krolik, J. H. 2004, *ApJS*, 155, 675
- Kallman, T., Evans, D. A., Marshall, H., et al. 2014, *ApJ*, 780, 121
- Kramida, A., Ralchenko, Yu., Reader, J., and NIST ASD Team (2014). NIST Atomic Spectra Database (ver. 5.2), [Online]. Available: <http://physics.nist.gov/asd> [2014, November 19]. National Institute of Standards and Technology, Gaithersburg, MD.
- Liang, G. Y., Whiteford, A. D., & Badnell, N. R. 2009, *A&A*, 500, 1263
- Liang, G. Y., & Badnell, N. R. 2010, *A&A*, 518, AA64
- Liang, G. Y., Li, F., Wang, F. L., et al. 2014, *ApJ*, 783, 124
- Porquet, D., & Dubau, J. 2000, *A&AS*, 143, 495
- Rose, S. J. 1998, *Journal of Physics B Atomic Molecular Physics*, 31, 2129
- Rose, S. J., van Hoof, P. A. M., Jonauskas, V., et al. 2004, *Journal of Physics B Atomic Molecular Physics*, 37, L337
- Salzmann, D. 1998, *Atomic Physics in Hot Plasmas* (New York:Oxford Univ.Press)
- Salzmann, D., Takabe, H., Wang, F., & Zhao, G. 2011, *ApJ*, 742, 52
- Wang, F., Salzmann, D., Zhao, G., & Takabe, H. 2011, *ApJ*, 742, 53